Physics – Uspekhi **68** (8) 807 – 822 (2025)

CONFERENCES AND SYMPOSIA

PACS numbers: **07.87.+v, 96.60.–j**

ON THE 100th ANNIVERSARY OF S.I. SYROVATSKII'S BIRTH

Space-based and extra-atmospheric studies of the Sun*

V.D. Kuznetsov

DOI: https://doi.org/10.3367/UFNe.2025.03.039920

Contents

Abstract. Studies in solar physics were in the sphere of the scientific interests of S.I. Syrovatskii covering a wide range of problems, and the goal of these studies was to obtain a unified picture of physical processes on the Sun. Observations from spacecraft provide more and more detailed information about the phenomena and processes occurring on the Sun, stimulating the construction of physical models and giving a deeper understanding of how the Sun is structured and how it works. An overview of space-based and extra-atmospheric studies of the Sun is given, covering all layers of the solar atmosphere from the convective zone and the photosphere to the solar corona and solar wind.

Keywords: Sun, space-based research, magnetic fields, flares, solar wind

1. Introduction

Within the wide range of scientific interests of S.I. Syrovatskii in the field of space physics and plasma physics, the last years of his life were devoted to research in solar physics. Based on the theory of current sheets in highly conductive plasma with a strong magnetic field [1] developed by him, he proposed a mechanism for converting magnetic field energy into plasma heating and radiation, which received both experimental (laboratory) [2, 3] and observational confirmation using solar flares as an example (see below). S.I. Syrovatskii supervised studies of the formation and evolution of current sheets (see [1] and references therein), the nature of solar flares [4, 5], oscillatory convection in a strong magnetic field [6], the secondary effects of solar flares [7, 8], the problem of particle acceleration [4], the solar dynamo [9, 10], magnetic fields on the Sun [11, 12], the possibility of detecting current sheets in the solar atmosphere [13, 14], etc. The Sun, as a natural plasma laboratory, the closest of all astrophysical objects, is studied in most detail using ground-based and space observations, and in recent decades the most significant achievements in the study of the Sun have been achieved using space-based research. The 'golden age' of solar physics in space [15, 16], which was marked by the launch of a series of innovative space missions (Yohkoh, SOHO, etc.) in the 1990s, continues, since, along with existing solar space missions (SOHO, Hinode, STEREO, SDO, IRIS, etc.), new ones have been launched (Parker Solar Probe, Solar Orbiter, CHASE, ASO-S, Aditya-LL, Proba-3, etc.), designed to provide researchers with the best up-to-date data for solving such urgent problems of solar physics as the mechanisms of heating the solar corona and acceleration of the solar wind, the fine and ultrafine structure and dynamics of the solar atmosphere, trigger mechanisms of the most powerful manifestations of solar activity, flares and coronal mass ejections, the acceleration of particles and their propagation in the corona and heliosphere, the structure and dynamics of magnetic fields in the polar regions of the Sun, the dynamo mechanism and the solar cycle, and the properties of plasma turbulence.

2. Concept of space-based research on the Sun

The modern concept of space-based research on the Sun includes observations of the Sun from close distances, from out-of-ecliptic positions, from favorable heliopositions (Lagrange points L1, L5, etc.), from near-earth orbits with high spatial resolution, as well as from extra-atmospheric rockets and stratospheric balloons (Fig. 1).

The Table shows completed and active solar space missions of various space agencies. Among the implemented extra-atmospheric rocket observations of the Sun, we can mention

V.D. Kuznetsov
Pushkov Institute of Terrestrial Magnetism, Ionosphere and Radio Wave Propagation, Russian Academy of Sciences, Kaluzhskoe shosse 4, 108840 Troitsk, Moscow, Russian Federation
E-mail: kvd@izmiran.ru

Received 30 June 2025
Uspekhi Fizicheskikh Nauk **195** (8) 858 – 874 (2025)
Translated by V.L. Derbov

* The review is based on a talk given at the Scientific Session of the Physical Sciences Division of the Russian Academy of Sciences on 5 March 2025 (see *Phys. Usp.* **68** (8) 745 (2025); *Usp. Fiz. Nauk* **195** (8) 793 (2025)).

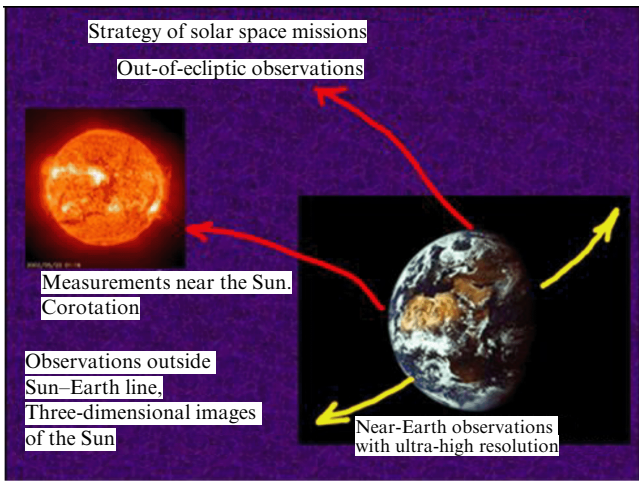

Figure 1. Illustration of strategy of solar space missions.

the NASA (National Aeronautics and Space Administration, USA) experiments EUNIS (Extreme Ultraviolet Normal Incidence Spectrograph) (launched in 2006, 2007, 2013), Hi-C (High resolution Coronal imager) (launched in 2012), and VAULT (Very high Angular resolution ULtraviolet Telescope) (launched in 2014), and the NASA balloon experiment together with Spain and Germany, SunRise IMAX (Imaging Magnetograph eXperiment) (launched in 2014).

Observations and local measurements near the Sun allow us to relate phenomena in the solar atmosphere with those in the corona and solar wind. Small-scale structures in the solar corona, pulled by the solar wind from their sources on the solar surface, move away from the Sun at different speeds, they collide and merge, and turbulence arises, which leads to mixing of disturbances and structures coming from the Sun and to their disappearance and loss of information about their origin on the Sun [17]. The Parker Solar Probe and Solar Orbiter spacecraft, moving along heliocentric orbits, are periodically at distances from the Sun where measurements of unblurred small-scale structures of the solar wind directly related to its sources on the surface of the Sun are possible. Observations with high spatial resolution near the Sun make it possible to study the fine structure and dynamics of the solar photosphere and transition region as a basis for understanding the heating mechanism of the solar corona, the origin of the solar wind, and trigger mechanisms of solar flares and mass ejections, and to observe weak energy-release events (micro- and nano-flares) that are not visible from Earth. The heliocentricity of orbits during the approach of spacecraft to the Sun, as well as observations from spacecraft outside the Sun–Earth line (STEREO project), make it possible to periodically observe the side of the Sun that is not visible from Earth, which makes it possible to monitor activity on this side and is important for early prediction of space weather. Continuous observations of the Sun at the L1 Lagrange point (SOHO, Aditya-L1 projects) make it possible to obtain operational information on the state of the Sun's activity, such as active regions, flares, and mass ejections, which is used to study and monitor space weather, including the study and prediction of extreme events in the Sun–Earth system.

Out-of-ecliptic observations of the Sun (Solar Orbiter project) and local measurements in the corona and heliosphere are aimed at studying polar magnetic fields and phenomena, which will provide a better understanding of

Table. Solar space projects. Launch year and years of operation of completed missions are indicated in parentheses.

Completed	ULYSSES (1990–2009) (NASA) Yohkoh (1991–2001) (JAXA/ISAS) CORONAS-I (1994–2001) (Roskosmos) TRACE (1998–2010) (NASA) CORONAS-F (2001–2005) (Roskosmos) RHESSI (2002–2018) (NASA) CORONAS-FOTON (2009) (Roskosmos)
Active	Voyager-1, 2 (1977) (NASA) Wind (1994) (NASA) SOHO (1996) (ESA, NASA) ACE (1997) (NASA) Hinode (2006) (JAXA, NASA) STEREO-A, B (2006) (NASA) IBEX (2008) (NASA) SDO (2010) (NASA) IRIS (2013) (NASA) DSCOVR (2015) (NASA) Parker Solar Probe (2018) (NASA) Solar Orbiter (2020) (ESA, NASA) CHASE (Xihe-1) (2021) (NJU et al.) ASO-S (2022) (CAS) Aditya-L1 (2023) (ISRO) Proba-3 (2024) (ESA)

Abbreviations and websites of the projects:
ULYSSES (https://science.nasa.gov/mission/ulysses/)
Yohkoh (https://www.isas.jaxa.jp/en/missions/spacecraft/past/yohkoh.html, https://science.nasa.gov/mission/yohkoh/)
TRACE — Transition Region And Coronal Explorer (https://science.nasa.gov/mission/trace/)
CORONAS — Coronal Orbital Near-Earth Observations of the Sun (http://coronas.izmiran.ru/)
Voyager-1, 2 (https://science.nasa.gov/mission/voyager/)
Wind (https://wind.nasa.gov/)
SOHO — SOlar and Heliospheric Observatory (https://www.esa.int/Science_Exploration/Space_Science/SOHO)
ACE — Advanced Composition Explorer (https://science.nasa.gov/mission/ace/)
RHESSI — Reuven Ramaty High Energy Solar Spectroscopic Imager (https://science.nasa.gov/mission/rhessi/)
STEREO — Solar TErrestrial RElations Observatory (https://stereo.gsfc.nasa.gov/)
IBEX — Interstellar Boundary Explorer (https://science.nasa.gov/mission/ibex/)
SDO — Solar Dynamic Observatory (https://sdo.gsfc.nasa.gov/)
IRIS — The Interface Region Imaging Spectrograph (https://iris.gsfc.nasa.gov/)
DSCOVR — Deep Space Climate Observatory (https://science.nasa.gov/mission/dscovr/)
Parker Solar Probe (PSP) (https://science.nasa.gov/mission/parker-solar-probe/)
Solar Orbiter (SolO) (https://www.esa.int/Science_Exploration/Space_Science/Solar_Orbiter)
CHASE — Chinese Hα Solar Explorer (https://ssdc.nju.edu.cn/home)
ASO-S — Advanced Space-based Solar Observatory (http://aso-s.pmo.ac.cn/en_index.jsp)
ESA — European Space Agency (https://www.esa.int/)
NASA — National Aeronautics and Space Administration (https://www.nasa.gov/)
JAXA — Japan Aerospace Exploration Agency (https://global.jaxa.jp/)
ISAS — Institute of Space and Astronautical Science (https://www.isas.jaxa.jp/en/)
CAS — Chinese Academy of Science (https://english.cas.cn/)
NJU — Nanjing University
ISRO — Indian Space Research Organization (https://www.isro.gov.in/)
Aditya-L1 (https://www.isro.gov.in/Aditya_L1.html)
Proba-3 (https://www.esa.int/Enabling_Support/Space_Engineering_Technology/Proba_Missions/Proba-3_Mission3)

the process of field reversal in the solar cycle and the solar dynamo, the origin of the fast solar wind, coronal holes, and polar mass ejections. Observations of the ecliptic corona and streamer belt, as well as the heliolongitudinal extent of coronal mass ejections, will also become possible.

Observations from the Earth orbit (Hinode, SDO, IRIS, ASO-S, Proba-3 projects, rocket and balloon experiments) are possible with super-high spatial resolution and with the transmission of a large volume of information to Earth, which makes it possible to study rapidly dynamic phenomena in the solar atmosphere (SDO project).

Observations from heliocentric orbits in the ecliptic plane outside the Sun–Earth line from two STEREO spacecraft make it possible to monitor disturbances coming from the Sun in the direction of Earth, determine their shape and extent, and see the state of activity in areas of the solar disk invisible from Earth, thus providing key information for studying and forecasting space weather.

A review of some previously obtained results of space studies of the Sun can be found in Refs [18–23].

Several new solar space projects have been launched recently (see Table). We provide brief information about some of them.

In the Parker Solar Probe project [24], the spacecraft, due to multiple gravitational maneuvers near Venus, approached the Sun to a record-breaking distance of 9.5 solar radii, conducting local measurements of the corona and solar wind, as well as observing the corona from the inside using an optical camera. A complex of scientific equipment consisting of devices for local measurements of electric and magnetic fields, energetic particles (He-3, He-4, etc.), electrons, alpha particles, and protons in the solar wind, as well as a wide-angle camera, is intended to study the structure and dynamics of magnetic fields in sources of fast and slow solar wind, identify energy flows that heat the corona and accelerate the solar wind, determine the mechanisms of acceleration and transport of energetic particles, and study dusty plasma in near-solar space and determine its influence on the generation of solar wind and energetic particles.

In the Solar Orbiter project [25], the spacecraft, through multiple maneuvers near Venus, approached the Sun to a distance of 60 solar radii, after which the spacecraft will gradually tilt its orbit to 24°–33° relative to the ecliptic plane. The scientific equipment complex (SEC) of the project consists of ten instruments, six of which are constantly directed at the Sun (polarimetric and helioseismic telescope, hard ultraviolet telescope, X-ray spectrometer/telescope, instrument for spectral imaging of the coronal environment, coronagraph, heliospheric telescope), and four instruments (solar wind plasma analyzer, energetic particle detector, magnetometer, radio and plasma wave analyzer) conduct local measurements of the environment around the spacecraft, making it possible to solve a wide range of problems from the inner layers of the Sun to the corona and solar wind, such as the action of the dynamo and modulation of the solar cycle, the relationship of the Sun with the heliosphere, heating of the corona, the formation and acceleration of the solar wind, and the generation of energetic particles and their propagation in the heliosphere.

In the CHASE (Xihe-1) project [26], using the Hα Imaging Spectrograph (HIS) with high spatial resolution (1.2″), spectral resolution (0.024 Å), and speed (tens of seconds), for the first time, full-disk spectroscopic images of the Sun in the Hα range (spectral lines SiI (6560.6 Å), Hα (6562.8 Å) and FeI (6569.2 Å)) have been obtained, equivalent to 'computer tomography' of the lower layers of the Sun's atmosphere — the photosphere and chromosphere. Such observations significantly complement observations by the current SDO, IRIS, STEREO, PSP, SolO, and ASO-S missions and make it possible to study the dynamics of the photosphere and chromosphere and the mechanisms of eruptive phenomena, flares, rotation of the solar atmosphere, and mass and energy transfer in the atmospheric layers.

In the ASO-S project [27], the spacecraft was launched into a near-Earth sun-synchronous orbit (altitude 700–750 km) to study photospheric magnetic fields, flares, mass ejections, and their relationships with each other. The SEC consists of three instruments: a full-disk vector magnetograph, a full-disk La telescope, and a hard X-ray telescope.

In the Aditya-L1 project [28], the spacecraft is placed in orbit around the L1 Lagrange point with seven instruments on board: a coronagraph, an ultraviolet telescope, a soft and hard X-ray spectrometer, two solar wind particle analyzers, and a magnetometer. Studies of the dynamics of the photosphere, chromosphere, and corona of the Sun, observations of coronal loops and mass ejections, flares, magnetic fields in the solar corona, and the solar wind are aimed at better understanding solar activity mechanisms, solving the problem of anomalous heating of the corona and improving space weather prediction.

In the Proba-3 technology project [29], two spacecraft in a near-Earth highly elliptical orbit form a giant space coronagraph (with a field of view of 1.08–3 solar radii) — an artificial solar eclipse when one spacecraft carries a telescope and the other acts as an eclipsing disk (Fig. 2). High spatial resolution and clarity of images of the inner corona will make it possible to study in detail the fine magnetoplasma structure of the inner corona, mass and energy transfer, heating of the corona, and the formation and acceleration of the solar wind. The SEC also includes a radiometer for measuring the radiation flux from the Sun and a spectrometer for recording energetic electrons in Earth's radiation belts.

Observations of the Sun by spacecraft are supplemented by extra-atmospheric observations on rockets and stratospheric balloons, which make it possible to exclude the influence of the atmosphere and obtain information about the Sun in the ultraviolet and X-ray ranges of the spectrum. Such observations, as a rule, are aimed at solving a limited range of problems from among the most significant problems of solar physics that can be solved by such observations.

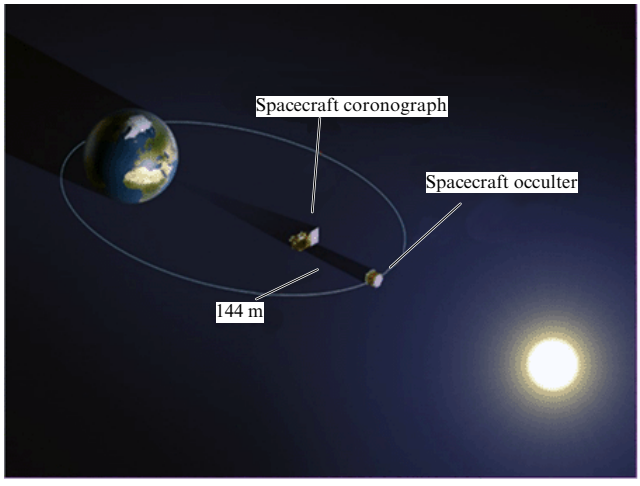

Figure 2. Schematic diagram of space coronagraph in Proba-3 project (adapted from [29]).

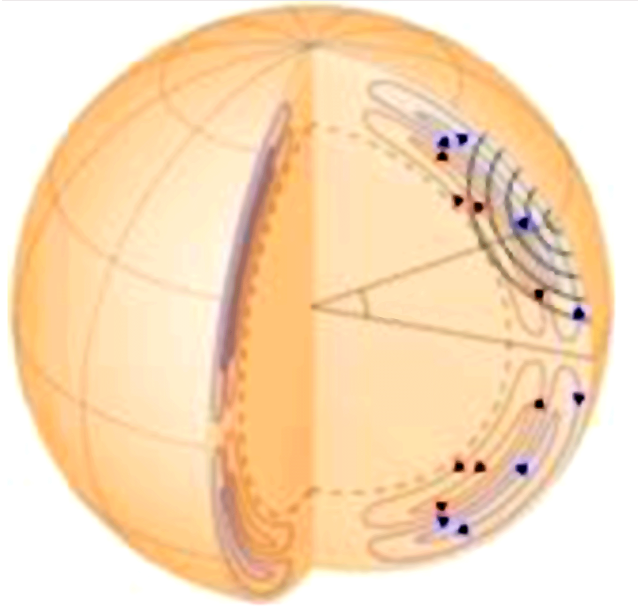

Figure 3. Schematic representation of profile of two-cell meridional circulation in convective zone [31] (http://hmi/stanford/edu/hminuggets/7p = 5).

3. Interior of the Sun

The study of the interior of the Sun, which is important for understanding the operation of the solar dynamo and the solar cycle, is continuing on the SDO [30] with the Helioseismic and Magnetic Imager (HMI). Based on the analysis of helioseismic data [31], as we have already noted earlier, indications have been obtained of a two-cell meridional circulation in the convective zone of the Sun, which plays an important role in the transfer of magnetic fields in the solar activity cycle (Fig. 3). A poleward meridional flow of 15 m s^{-1} extends in the convection zone at depths from the photosphere to $\sim 0.91R_\odot$, and a flow towards the equator of about 10 m s^{-1} is found in the convection zone between 0.82 and $0.91R_\odot$. In the convection zone below $0.82R_\odot$, the meridional flow is again poleward, indicating a second meridional circulation cell beneath the surface cell.

Kinematic theories of the dynamo generally assume the presence of a single meridional circulation cell in the convection zone with an equatorial flow along its bottom. The application of the dynamo model with flow transfer, which in the case of single-cell meridional circulation was used to describe many important observational details of the solar cycle, to the case of multi-cell meridional circulation (Fig. 4)

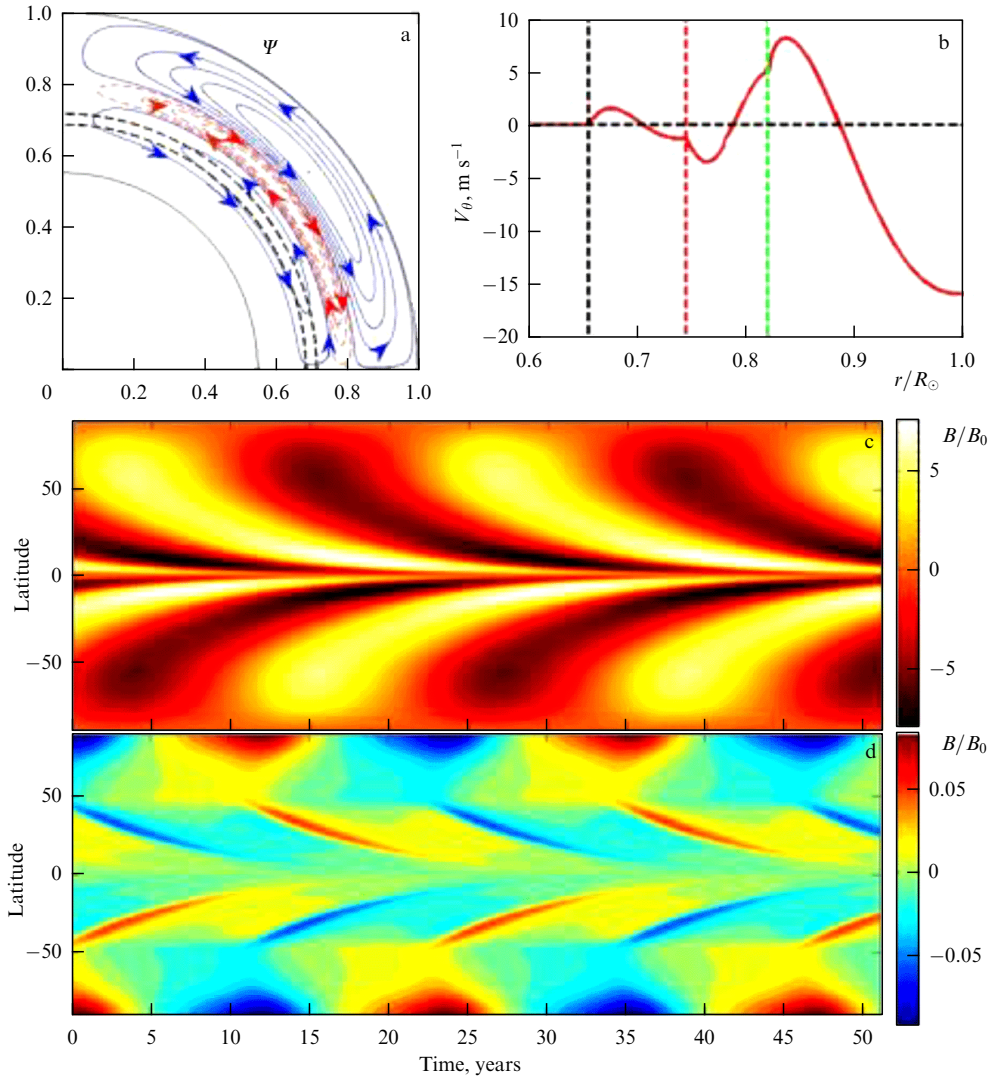

Figure 4. Reproduction of butterfly diagrams within framework of dynamo model with flux transfer for meridional flow toward equator along bottom of convective zone [32] (https://iopscience.iop.Org/article/10.1088/0004-637X/782/2/93).

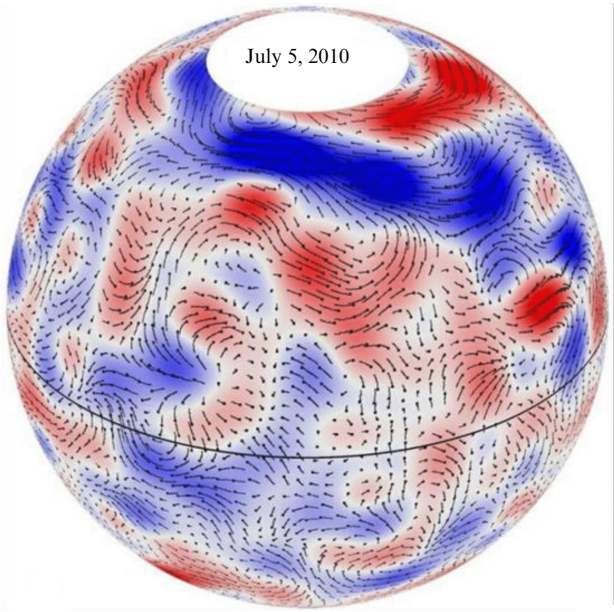

Figure 5. Giant convective cells on the Sun [33] (https:// www.nasa.gov/missions/sdo/nasa-astrophysicist-confirms-existence-of-giant-convection-cells-on-sun/).

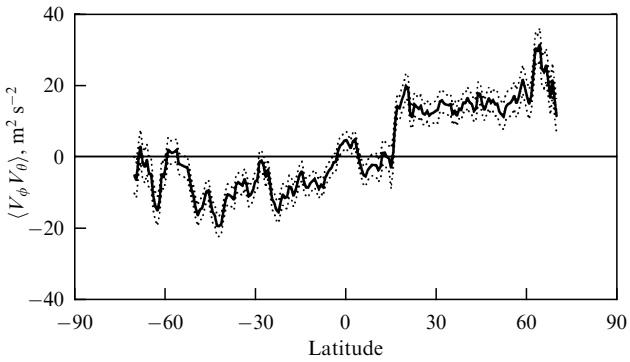

Figure 6. Latitudinal distribution of Reynolds stresses produced by giant cells, showing transport of angular momentum toward equator and requiring its faster rotation [33].

showed that observations in the form of corresponding 'butterfly' diagrams can be reproduced only when additional cells of the meridional circulation are arranged at the bottom so that there is an equatorward flow at the bottom of the convective zone, i.e., there must be an odd number of cells along the depth of the convective zone [32].

The analysis of giant convective cells based on HMI/SDO Doppler data (Fig. 5) made it possible to understand why the Sun's equator rotates faster than its polar regions. The calculated picture of the latitudinal distribution of Reynolds stresses (Fig. 6) associated with flows in the discovered giant cells showed that the transfer of angular momentum in both hemispheres occurs toward the equator, and this ensures the maintenance of a faster rotation of the Sun's equator than that of the polar regions (the rotation period being 24 days at the equator and 35 days near the pole) [33].

4. Solar atmosphere between photosphere and corona

The region of the solar atmosphere, including the photosphere, chromosphere, transition region, and lower corona, is

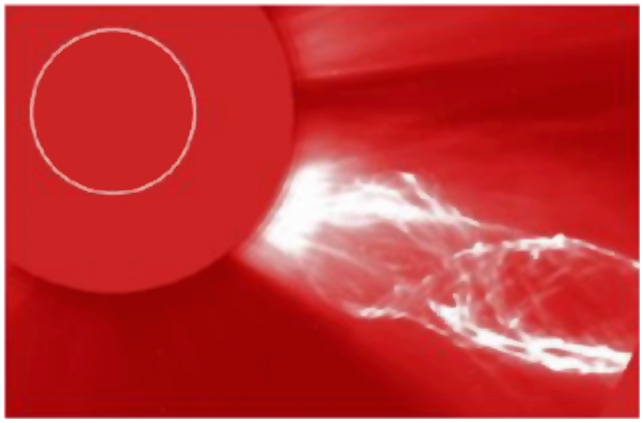

Figure 7. Unwinding magnetic tube in mass ejection according to LASCO/SOHO data [34].

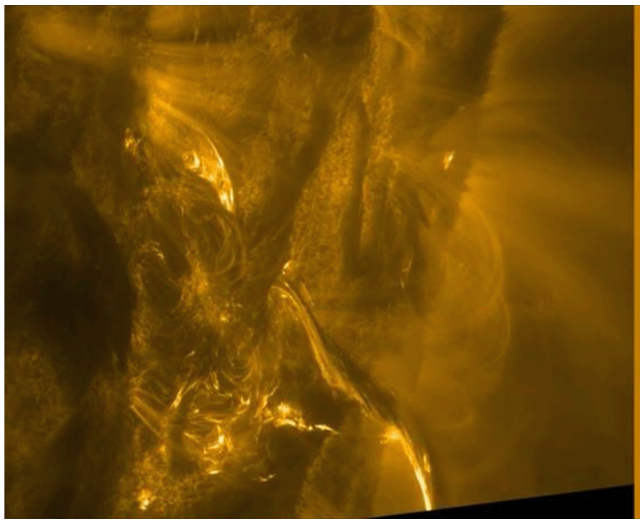

Figure 8. Detail of Solar Orbiter movie (2503_008_AR_EN.mp4) demonstrating spinning up of highly twisted magnetic tube [25].

the most difficult to study due to its nonstationarity and nonequilibrium caused by the continuous action of convection and the emergence of magnetic fluxes of different scales from under the photosphere. It is in this region that processes occur that are responsible for the origin of flares and mass ejections and for the heating of the solar corona, and a fine structure is formed that determines the sources of the solar wind outflow. Special projects are aimed at studying the transition region between the photosphere and the corona, within the framework of which high spatial, temporal, and spectral resolution is ensured (Hi-C, IRIS, VAULT, etc.).

Numerous observations of magnetic fields in the solar atmosphere with high spatial resolution (TRACE, SOHO, Hinode, SDO, Solar Orbiter, etc.) indicate their strong twisting, acquired in the subphotospheric layers and manifested in such phenomena as flares and mass ejections. In films obtained within the framework of the above-mentioned missions, one can see how twisted magnetic tubes (bundles) unravel when they are injected in the upper atmosphere (Figs 7, 8), and this twisting, reaching certain critical values, is considered one of the trigger mechanisms of the observed eruptive phenomena.

Using high-precision observations with the IMAX solar magnetograph (polarimeter) in the Sunrise mission on a

stratospheric balloon with a record-breaking spatial resolution (100 km on the solar surface), the formation and evolution of isolated magnetic tubes, which are considered to be the fundamental magnetic building blocks of the solar photosphere, were tracked in detail for the first time [35]. The observed physically complex process was characterized by many phenomena: the emergence of a magnetic loop, the expulsion of its bases from the granule, the merging of magnetic flux elements into a long-lived magnetic flux, the formation of a magnetic element with a kilogauss magnetic field strength through convective collapse and granulation compression, and subsequent weakening of the field strength with a further increase to kilogauss values, due to either oscillations or secondary collapse. The observational properties of convective-driven vortex flows detected on a quiet disk are described using magnetograms, Dopplergrams, and IMAX images. The vortex density is about 3.1×10^{-3} vortices/(Mm^2 min) with an average duration of individual events of 7.9 min. Repeating vortices are detected in the same places; typical vorticities correspond to a rotation period of about 35 min, with a preferred counterclockwise rotation, which is presumably associated with vorticity due to differential rotation of the Sun [36].

The Hinode observations revealed the strongest magnetic field ever measured on the solar surface, 6250 G. This superstrong magnetic field was formed as a result of the outflow of gas from one sunspot pressing on another, and it was located in the bright region between two sunspot shadows [37].

In Ref. [38], coronal voids were studied based on Solar Orbiter observations — extended regions of the quiet solar atmosphere, which, according to observations in the hard ultraviolet (UV) range, are characterized by weak radiation compared to the surrounding quiet corona. Such voids are defined by the intensity threshold, which is taken to be equal to 75% of the average intensity of hard UV radiation for the quiet Sun, recorded by the high-resolution channel of the Extreme Ultraviolet Image (EUI) telescope. A comparison of photospheric magnetic fields under coronal voids with magnetic fields of the quiet Sun was carried out based on observations by the High Resolution Telescope (HRT) of the Polarimetric and Helioseismic Imager (PHI). The sizes of the studied voids varied from several granules to several supergranules and on average had a reduced intensity of 67% of the average value of the entire field of view. The magnetic flux density in the photosphere below the voids was 76% (or more) lower than in the surrounding quiet Sun. It was noted that, in coronal voids, network structures are weakly manifested or completely absent. It was concluded that coronal voids are formed due to locally reduced heating of the corona with reduced magnetic flux density in the photosphere, which makes them a separate class of dark structure that differs from coronal holes.

Using Dopplergrams of the entire solar disk obtained by CHASE, the rotation curves of various layers of the photosphere and chromosphere were analyzed. A new pattern in the rotation of the solar atmosphere was discovered, consisting of an increase in the rotation velocity with altitude, which raises the question of the physical mechanism of this phenomenon, since usually, due to the action of viscous forces, the rotation velocity decreases with altitude [39]. For example, at the equator, the rotation velocity increases from 2.81 ± 0.02 rad s^{-1} at the bottom of the photosphere to 3.08 ± 0.05 rad s^{-1} in the chromosphere. One of the reasons for the discovered rotation pattern may be the ubiquitous small-scale magnetic fields and the altitude-dependent degree of their freezing into the solar plasma.

Wave processes in solar magnetic pores, intense concentrations of the magnetic field, were studied based on Solar Orbiter observations (HRT, PHI instruments) [40]. A combination of different measurements and methods was used to comprehensively diagnose MHD waves in pores in the form of bending modes and sausage modes, and a previously unobserved corrugation mode ($m = 2$) was identified in one of the most magnetically isolated pores. It was found that the most energetic mode in all four observed pores (i.e., the mode with the largest eigenvalue) was the sausage mode with a frequency in the range of 1.5–3.0 mHz, while bending modes identified in a slightly smaller frequency range of 1.4–2.3 mHz were the second most energetic empirical mode (i.e., with the second largest eigenvalue). Their frequencies are slightly lower than those of the bending modes identified as the third empirical mode (in the range from 1.8 to 2.7 mHz). Close frequencies in the identified modes of MHD waves may indicate that they are related to each other, and the observed large variations in the pore area, up to $40 \pm 10\%$, may indicate a nonlinear regime. Since the identified second and third spatial mode are bending modes with perpendicular oscillation directions, they may be of interest in connection with the search for manifestations of torsional Alfvén waves in the solar atmosphere, considered to be possible sources of solar corona heating, the detection of which, however, is difficult in all layers of the solar atmosphere due to their incompressible nature — they do not cause changes in the radiation intensity. Further analysis of higher resolution observations (in particular, during the flight of the SUNRISE solar observatory installed on a balloon and during the Solar Orbiter approach to the Sun) is planned.

In Ref. [41], using observations by three Solar Orbiter instruments (EUI HRIEUV, PHI HRT, and SPICE), signs of propagation of torsional motion in the corona were detected that are compatible with the interpretation of either propagating torsional Alfvén waves in the low coronal structure or unwinding of the magnetic bundle. The propagation velocity of the observed motions was from 136 km s^{-1} to 160 km s^{-1}, which is consistent with the expected Alfvén velocities. The observed rotational motions in the transverse direction with velocities of 26 km s^{-1}–60 km s^{-1} also indicate the presence of torsional waves, and their amplitude, which is approximately 30% of the local Alfvén velocity, indicates a nonlinear regime of such waves. One of the main features of these oscillations is their significant amplitude. The question of the source of these oscillations remains open. In the case under consideration, the torsional waves were caused by magnetic reconnection, which, as noted earlier [42, 43], can lead to a twisting of the plasma motion.

The high dynamics of the chromosphere, established by Hinode observations, plays an important role in heating the solar corona and mass transfer to the solar wind, and it manifests itself in the form of plasma eruptions around sunspots upward to the corona, in the form of small and sporadic plasma jets (Fig. 9).

Along the detected type II spicules [45], the chromospheric plasma is injected into the upper atmosphere at velocities of the order of 50–100 km s^{-1}; however, tracking the process of mass and energy transfer into the corona is difficult due to their extinction, small size ($< 0.5''$), and short

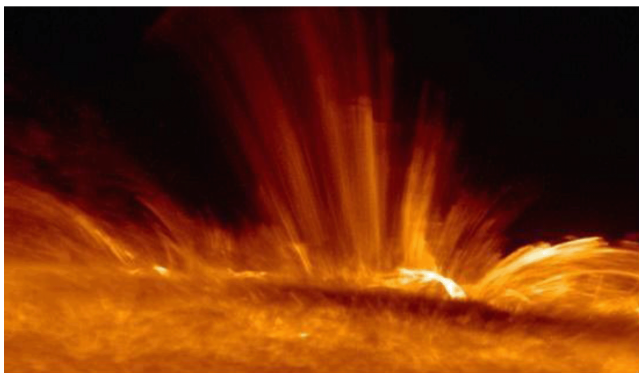

Figure 9. Dynamically active chromosphere [44] (©NAOJ/JAXA).

lifetime (10–20 s) [46]. The phenomena that were observed in the transition region and lower corona using high-resolution Hi-C telescopes (bright dots) [47], IRIS and SDO (propagating coronal disturbances) [48] are considered possible coronal 'twins' of type II spicules, but more detailed correlated observations of the chromosphere and the transition region of the lower corona with high temporal and spatial resolution are needed to identify them. Modeling of type II spicules within the framework of radiation magnetohydrodynamics using observational data from IRIS and the VAULT2.0 rocket experiment made it possible to clarify some features of the processes occurring in type II spicules, in particular, the observation of velocities up to 300 km s^{-1} [49, 50]. The spicule matter exists in suspension high in the atmosphere, but at lower temperatures (observed in Lyα), until it is heated and becomes visible at transition region temperatures as a jet. Heating begins lower in the spicules, and a rapid propagation of a thermal front occurs. This front is observed as rapid motion in the picture plane, containing pre-existing spicules inside. Thus, it is concluded that the high velocities in spicule jets should not be perceived as real massive upward plasma flows, but only as apparent velocities of a rapidly propagating thermal front along previously existing spicules.

The small IRIS spacecraft with a UV imaging spectrograph of high spatial ($0.33''-0.4''$) and temporal (2 s) resolution and a wide spectral range provides simultaneous spectra and images (field of view: $175'' \times 175''$) of the photosphere, chromosphere, transition region, and corona. Analysis of the obtained images and spectra showed a wide variety of ongoing processes, among which are the braiding of magnetic field lines and magnetic reconnection, the interaction of active regions with the magnetic field of the chromospheric network and small-scale fields of the magnetic carpet, the interaction of emerging magnetic fluxes with fields in the overlying atmosphere, rapidly flaring and fading UV spots reflecting energy transfer in the solar atmosphere, the generation and propagation of various types of waves and their conversion, the acceleration of nonthermal particles, the mass flow into the corona and the solar wind, and coronal processes in the form of heat conductivity or energetic particles [51].

Using the data from Hi-C telescope rocket observations in the UV range of the spectrum with high spatial resolution, new results were obtained concerning the transition region and the lower corona. In Ref. [52], using Hi-C data and MHD modeling, a study was conducted of the turbulent relaxation of solar coronal loops containing entanglement of field lines, which is considered one of the mechanisms for the release of magnetic energy and heating of the solar corona. When studying the issue of observational manifestations of energy release in such entangled magnetic structures, it was established that the observational manifestations depend on the degree and nature of the entanglement of field lines in the loop and do not always reflect the braiding of field lines. A uniformly heated loop, without visible filamentary structures, is formed with strong entanglement of field lines in the loop and with uniform (across the loop) turbulence associated with the release of energy. The intertwined structures identified in the Hi-C observations [53] manifest themselves in loops containing large structures such as coherent flux tubes, separatrices, leading to increased heating on some filamentary structures with less heating on others.

Substructures in the form of miniature loops about 10^8 cm long and less than 2×10^7 cm thick have been discovered in coronal loops. Such mini loops can be interpreted as coronal manifestations of small magnetic tubes emerging from beneath the photosphere with a distance between the bases of the tubes on the photosphere corresponding to the diameter of the granulation cell [54, 55]. The highest spatial resolution data ($0.47''$) of the lower corona and transition region, unattainable in other observations, were obtained during five-minute Hi-C2.1 rocket observations at a wavelength of 175 Å [56]. These data, along with other related observations, indicate the key role of the small-scale structure and dynamics in understanding the complex transition region between the photosphere and the corona. The most probable widths of filamentary structures with a low radiation level turned out to be close to ≈ 388 km, and a further increase in spatial resolution, as analysis shows, will make it possible to resolve the fundamental width of individual coronal filaments [57]. A number of new phenomena were also discovered using the Hi-C data: small-scale 'sparking' of dynamic bright points against the background of radiation from active regions in the form of moss [47], plasma counterflows in filaments [58], moving bright points and jets in the umbra of sunspots [59, 60], and the relationship of the glow in the lower corona and transition region with small-scale chromospheric dynamics in active regions [56].

The database of X-ray phenomena and micro- and nanoflares on the Sun for the analysis of the sources of heating of the solar corona was supplemented by high-sensitivity and high-spatial-resolution observations on the small spacecraft NuSTAR (Nuclear Spectroscopic Telescope Array) using a hard X-ray Sun-aimed telescope, designed to study black holes [61].

The high spatial resolution of the Hinode and SDO telescopes and spectroscopic measurements made it possible to observe and study current sheets in the solar atmosphere, the accumulation of magnetic energy in which and its release by magnetic reconnection play a key role in solar flares. Based on spectroscopic observations on Hinode and SDO, the formation, structure, and evolution of the current sheet, which arose as a result of the eruptive flare X8.3, were observed at the western edge of the Sun on September 10, 2017 (Fig. 10) [62]. During filament eruption, a bright region of radiation formed at the base of the eruption, corresponding to the high plasma temperature, which, after the flare, turned into a magnetic loop with a cusp-like shape at its top. From it, in the direction of the erupting filament, a long and narrow linear structure visible in the radiation was formed, which was accepted to be the current sheet in which magnetic reconnection occurs.

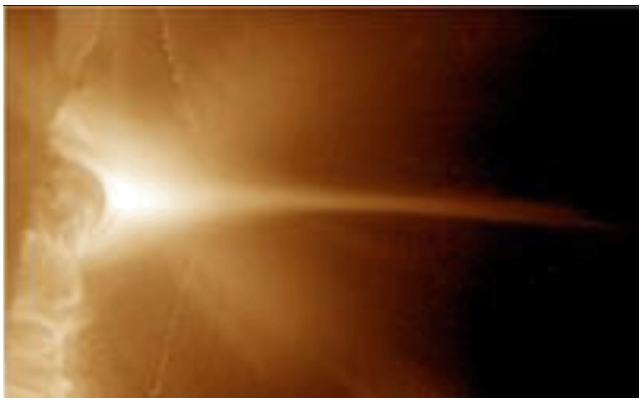

Figure 10. One of the fragments of current sheet image in the form of a bright linear structure emanating from cusp-like region [62].

The plasma temperature in the current sheet reached values of 15–20 million degrees and the range of its values is relatively narrow. The highest temperatures were observed after the flare at the base of the current sheet, in the region near the top of the arcade, and decreased with increasing height. The increase in intensity in the current sheet began at the lowest altitudes and propagated outward at a speed of about 288 km s^{-1}. A strong nonthermal broadening of the spectral lines was observed in the current sheet, corresponding to plasma velocities of 70–150 km s^{-1}, which increased with altitude and decreased with time, apparently reflecting flare-induced plasma motions. Measurements of radiation in different spectral channels allowed us to assume that the current sheet was formed from coronal plasma, and that plasma heating occurred in it with the release of energy during magnetic reconnection of the field lines entering the sheet. Observations of the current sheet of the solar flare SOL2017-09-10T16:06 [63] showed very high nonthermal velocities (up to 200 km s^{-1}) in the sheet, which allows us to assume that there are turbulent motions, and the layer has an internal thin and dynamic structure that promotes effective magnetic reconnection within it. The thickness of the current sheet is estimated in the range of $(7-11) \times 10^8$ cm. A detailed multiphase evolution of the current sheet at the early stages of a solar flare, including the stages of formation, quasi-stationary evolution, and destruction of the sheet, is described in [64] based on SDO observations. The magnetic structure in the vicinity of the current sheet at different stages of the evolution of a solar flare includes a high-temperature magnetic flux rope, supra-arcade plasma downflows, flare loops, a filament, and an erupting magnetic flux rope. The dynamics of the flare process and the phases of destruction of the current sheet are characterized by an increase in the size of cusp-like magnetic loops and stretching of the current sheet, subsequent growth of regular and ordered disturbances in the region between the current sheet and the flare arcade, the appearance of regular vortices growing for almost 10 min, and the disappearance of the current sheet in images in the 131-Å line, associated with its probable destruction. The features of current sheet observations and their characteristics were studied in Refs [65, 66] based on a large volume of SDO and SOHO data. For current sheets formed in the X-type configuration, during the magnetic reconnection period, the visible current sheet on the disk changed from a bright point to an elongated line, and the structure became thin at a late stage of reconnection. Subsequently, the plasma distribution in the current sheet manifested itself as a plasmoid chain. For the current sheet visible on the limb, its elongation occurred faster than on the disk, and a thinning process of the sheet was also observed. Even though the aspect ratio of the thickness and width of the current sheet for the limb cases is comparable to the critical theoretical value for the occurrence of the tearing mode instability, no obvious plasmoid chain was found inside these limb current sheets, and the density distribution was locally uniform. It is assumed that, due to the rapid elongation of limb current sheets, the tearing mode instability occurs very quickly, which is why tiny plasmoids are formed, the size of which is smaller than the resolution of the instrument. It is noted that the actual limb current sheet may be only a small segment of the visible bright beam, and not the entire beam. High-speed plasma flows that occur during solar flares in the processes of magnetic reconnection and the conversion of energy stored in the magnetic field into heat and plasma motion were first detected using spectroscopic observations on Hinode [44].

Using magnetic data from the SDO/HMI (Helioseismic and Magnetic Imager), it was possible for the first time to identify changes in magnetic fields on the surface of the photosphere (a decrease in the twisting of the field connecting two spots) caused by a flare, i.e., release of nonpotential energy of the magnetic field, and to obtain an answer to the long-standing question about the possibility of registering changes in the field on the photosphere during flares [67]. In Ref. [68], based on data from the Solar Orbiter/STIX HXR (STIX — Spectrometer/Telescope for Imaging X-rays), SDO/AIA (Atmospheric Imaging Assembly) and SDO/HMI, it was concluded that microflares accelerating electrons to high energies are localized in sunspots, which indicates the key role of strong magnetic fields in the efficient acceleration of high-energy electrons.

The first Aditya-L1 observations gave full-disk images of the Sun (photosphere and chromosphere) in the near ultraviolet range (200–400 nm) (Solar Ultraviolet Imaging Telescope (SUIT)), the use of which will make it possible to study the complex structure and dynamics of the magnetized solar atmosphere and to obtain constraints on the impact of solar radiation on Earth's climate [69]. Using the high-temporal and spectral resolution spectrometer HEL1OS/Aditya-LL (High Energy L1 Orbiting X-ray Spectrometer), X-ray spectra of the impulsive phase of solar flares and images of flares at low altitudes were obtained, inaccessible to observations by other observatories, which provides new information for understanding the explosive release of flare energy and electron acceleration during their pulsed phases [70–72].

ASO-S observations aimed at studying magnetic fields and their relationship with flares and mass ejections have made it possible to track and describe in detail a number of solar eruptions. Reference [73] describes the sympathetic eruption 13575 from the active region on February 9, 2024, in which characteristic elements of the event are highlighted: the occurrence of a class X3.4 flare from the primary eruption, a coronal mass ejection, and a wave visible in the hard ultraviolet; the wave leads to a high-amplitude transverse oscillation of the quiescent prominence, which loses its equilibrium and rises upward, setting in motion a second coronal mass ejection. Thus, an important role in the relationship between the primary eruption and the sympathetic eruption is played by the wave visible in the hard ultraviolet. In Ref. [74], the dynamics of multifilamentary eruptions is described based on the observations performed,

and a new mechanism for the eruption of filaments is presented, in which large-scale filaments are erupted by the action of small erupting filaments pushed from below. The initial kinetic energy of a large-scale eruption in this mechanism is obtained and transferred through other erupting structures. In Ref. [75], a detailed description of the morphology of coronal jets, which are a miniature version of large-scale eruptions, is given, and an assumption is made about the key role of sunspot rotation in the accumulation of free energy for flares and jets.

High-spatial-resolution observations on Hinode and IRIS made it possible to study wave motions in the prominence and to detect and identify observational manifestations of the resonant absorption of waves, which can play an important role in heating the solar corona. Resonant absorption between the transverse (Alfvén) waves observed by Hinode and the torsional waves observed by IRIS resulted in a turbulent flow that converted wave energy into heat, causing the prominence plasma temperature to increase from 10^4 K to 10^5 K [76]. Simulations using observational data also showed the emergence of turbulence due to resonant interaction of waves: Alfvén waves resonate with torsional motions in the surface layer of the filament, creating a semicircular flow of torsional disturbances that amplifies, becoming turbulent and converting wave energy into heat [77].

5. Corona and solar wind

The first Solar Orbiter images, obtained on June 15, 2020 by the hard X-ray telescope from a distance of 77 million km from the Sun, already made it possible to obtain the most detailed image of the full disk of the Sun and its corona and to identify numerous small flares, which were called 'solar fires' (Fig. 11) [25].

Solar Orbiter observations from close distances also made it possible to obtain detailed images and films of individual sections of the solar atmosphere and active regions and to see the complex structure of magnetic fields, their dynamics, small-scale mass ejection phenomena, etc. Figure 12 illustrates a detail from a film with the highest spatial resolution to date, in which the fine structure of the solar atmosphere is clearly visible: moss-like radiation identified with nanoflares, spicules, the ejection of a small twisted magnetic tube, coronal rain, etc. [25].

During the Solar Orbiter's approach to the Sun, observations near the Sun's south pole allowed identification of sources of fast and slow solar wind associated with tiny jets that are about 100 km wide and are visible in images as hair-like tufts that flare briefly (for about a minute) and eject charged particles at a speed of about 100 km s^{-1} (Fig. 13) [25, 78].

Figure 11. Detailed image of solar disk obtained by Solar Orbiter [25].

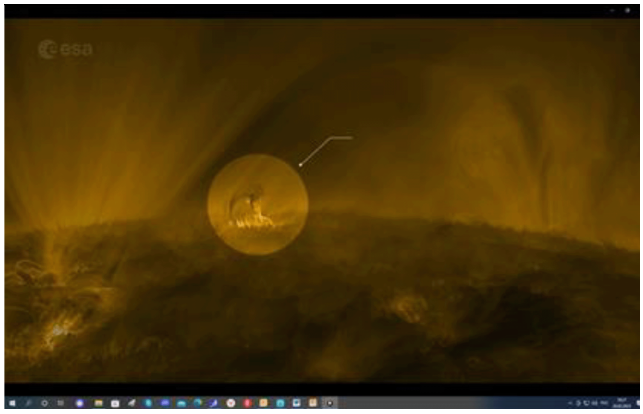

Figure 12. Image of section of solar atmosphere (detail of Solar Orbiter film) with highest spatial resolution to date, demonstrating fine structure and dynamics of solar atmosphere [25].

Such tiny jets have been shown to exist in all coronal holes in the Sun's atmosphere, and they are the source of both fast and slow solar wind. While the fast solar wind (speeds greater than 500 km s^{-1}) flows out from jets located directly in the coronal hole, a region of open field lines, the slow solar wind arises in regions with closed magnetic field lines bordering on

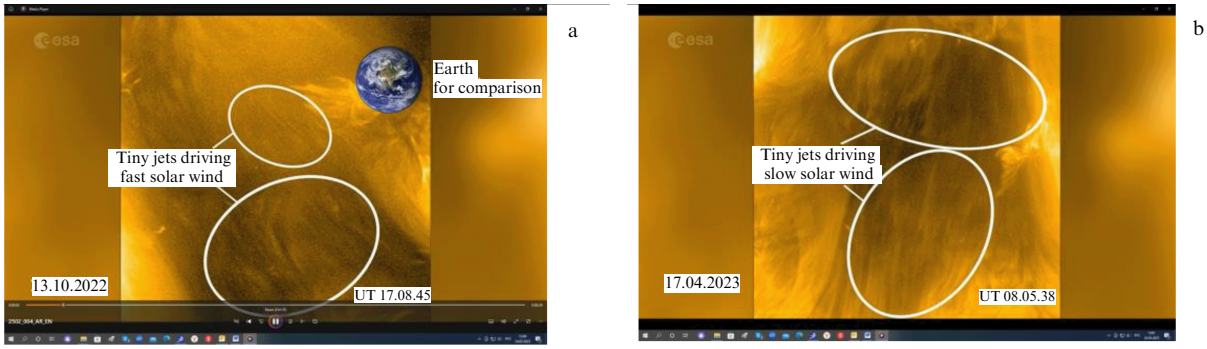

Figure 13. Detail of Solar Orbiter film demonstrating outflow of fast (a) and slow (b) solar wind from solar atmosphere [25].

regions of open field lines, where magnetic reconnection results in periodic breaks and reconnections of closed field lines, allowing plasma to escape from regions with closed field lines, forming nonuniform and nonstationary flows of the slow solar wind. A joint analysis of high-resolution remote sensing of tiny jets in coronal holes near the Sun's equator, obtained during approach to the Sun, and direct measurements of solar wind particles and the magnetic field made it possible to directly link the solar wind measured by the Solar Orbiter with the plasma flowing out of the observed jets. The analysis is based on a comparison of the content of magnesium, neon, and other heavy element ions in the solar corona, determined from remote observations, with their content in the solar wind, determined from local measurements. The content of these ions in the plasma of the solar corona differs significantly for different regions, which makes it possible to determine the region where a particular solar wind flow originated [79]. Similar conclusions about the origin of the slow solar wind based on observations with Solar Orbiter in magnetic reconnection processes at the edge of an active region were made in Ref. [80]. It should be noted that, previously, according to Hinode's observations, a continuous plasma outflow with a velocity of about 140 km s^{-1} from the edge of the active region with open magnetic field lines was detected in the active region of the corona adjacent to the equatorial coronal hole, identified as the source region of the low-speed solar wind [81].

The observed picture of the fast and slow solar wind origin, respectively, from coronal holes and from their border regions, where magnetic reconnection of open and closed magnetic field lines occurs, allows proposing a model in which coronal mass ejections and the fast and slow solar wind can be explained by a single, as yet unknown, source (driver) at the base of the solar corona. If in coronal holes the plasma along the field lines overcomes only the gravitational attraction, escaping into the corona in the form of a fast solar wind, and in the boundary regions of coronal holes it is additionally slowed down by the magnetic field, still escaping into the corona in the form of a slow solar wind, then, in the region of closed field lines, the action of the source should lead to tension of the closed magnetic configuration, the magnetic flux of which constantly decreases due to magnetic reconnection at its edges and is carried away into the slow solar wind. The same forces of the source that generate flows of fast and slow solar wind ultimately, due to a decrease in the magnetic flux of the closed magnetic configuration, push it upward, generating a coronal mass ejection. The characteristics of the mass ejection (speed, etc.) in this case should depend on the magnetic flux of the closed magnetic configuration, which is set in motion when the magnetic flux reaches a critical value.

Figure 14. Phenomenon of 'switchback' in solar corona — change in direction of magnetic field to opposite one [24].

Possible sources of these dynamic processes may be the gas pressure gradient and magnetic forces at the base of the corona, caused by heating processes (micro- and nanoflares) and the transfer of magnetic flux from the convective zone.

Local measurements by the Parker Solar Probe near the Sun (about 11 solar radii) made it possible to observe a phenomenon called 'switchback' or magnetic field reversal, when the magnetic field changes direction to the opposite, describing the shape of the letter S, as shown in Fig. 14 [82, 83]. One of the mechanisms for the formation of such structures is considered to be magnetic reconnection at the base of the corona between a system of open and loop structures emerging from beneath the photosphere (Fig. 15) [84]. In this model, switchback phenomena occur high in the corona, where coronal magnetic loops, anchored by their bases in the photosphere, experience magnetic reconnection when approaching open magnetic field lines in the solar wind, during which the magnetic field lines of the coronal loop are broken, and an S-shape of the field lines is formed. Along with this model, in which the observed bending of the field lines is formed due to magnetic reconnection, other models of the switchback phenomenon have been proposed [85], in which its occurrence is associated with such processes as magnetic reconnection with the formation of magnetic flux ropes [86] and current sheets [87], radial expansion of small Alfvén fluctuations of the solar wind [88], turbulence caused by shear movements at the boundary between fast and slow solar wind flows [89], reconnection between fast and slow solar wind, and overtaking of the slow wind by the fast wind [90].

Measurements of variations in the electron and proton velocity distribution functions aboard the Solar Orbiter [91] suggested that the observed 180°-bent magnetic field lines are reconnected to each other under the influence of the solar

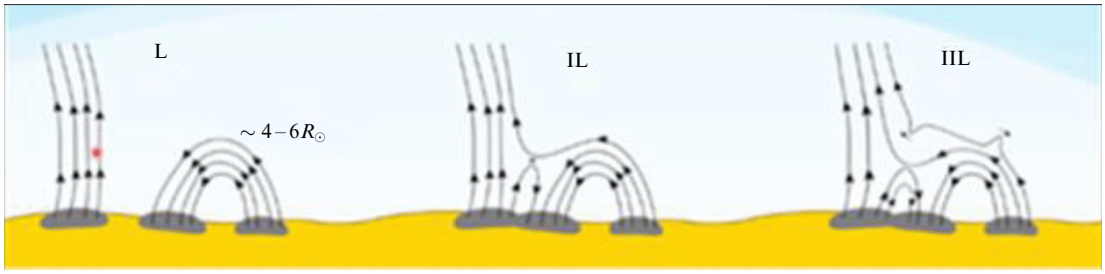

Figure 15. Magnetic reconnection at base of corona as possible source of formation of S-shaped magnetic field lines ('switchback') phenomena [66] (https://aasnova.org/2021/04/12/switching-it-up-with-solar-switchbacks/).

Figure 16. Coronal streamers visible as elongated bright elements during Parker Solar Probe flyby inside corona at distances between 50 and 35 solar radii (detail from film https://en.wikipedia.org/wiki/WISPR) [24]; Credit: NASA/Johns Hopkins APL/Naval Research Laboratory).

wind velocity shift, forming magnetic flux ropes, which may thus be surviving and modified remnants of 'switching events' occurring near the Sun. A study of the behavior of energetic particles with energies of 80–200 keV in the vicinity of S-shaped regions of the magnetic field yielded a constraint on the radius of curvature of the S-shaped bends of < 4000 km [92]. The high spatial resolution of the Solar Orbiter/Meris coronagraph made it possible to directly observe the energy release during the formation of the S-shaped force lines in magnetic reconnection and the upward and downward motion of plasma from the reconnection region characteristic of this process [25, 93]. Sudden and sharp reversals of the magnetic field in the heliosphere at different distances from the Sun, which are now called reverse switching phenomena, were previously reported based on the data from Helios-1 and Helios-2 [94], as well as ULYSSES [95, 96].

Moving in the solar corona, the Parker Solar Probe, using the WISPR (Wide-field Imager for Solar Probe) optical wide-angle camera, obtained for the first time images of coronal magnetic structures from inside the corona and repeatedly crossed them. They are coronal streamers (Fig. 16), magnetic loops and flux ropes, and mass ejections.

While crossing a coronal mass ejection at a distance of 10 million kilometers from the solar surface, the Parker Solar Probe observed turbulent vortices at the boundary of the ejection and the surrounding solar wind, caused by Kelvin–Helmholtz instability due to the difference in speeds along the boundary [24, 97]. By measuring variations in the brightness of the corona, the Parker Solar Probe observed for the first time the theoretically predicted effect of dust being swept out of the near-solar space by powerful coronal mass ejections with the formation of regions of dust voids and with subsequent rapid restoration of the dust distribution. The effect was observed at distances of up to 9.6 million kilometers from the Sun (1/6 of the distance from the Sun to Mercury). The discovered effect is important for predicting space weather, since interplanetary dust changes the shape and speed of the ejections, and its observation provides information about the ejections [24]. Based on observations of the corona by the WISPR camera, a translational tomography method is being developed for reconstructing three-dimensional images of the solar corona [98].

In Ref. [99], using the data of heliospheric magnetic measurements by the Parker Solar Probe and Solar Orbiter, directional discontinuities were studied, which are common structures in the solar wind plasma and one of the most important discontinuities along with shock waves. In the range of heliocentric distances of 0.06–1.01 AU, more than 140,000 discontinuities were detected, which were classified into subgroups of tangential discontinuities (TDs) and rotational discontinuities (RDs). It was found that the spatial density of discontinuities decreases with increasing radial distance from the Sun, and most of the discontinuities for which the normal component of the magnetic field is small are in fact TDs, regardless of the jump in the field amplitude. A study of the radial thickness evolution for TDs and RDs showed that the RD thickness decreases in the distance range from 0.06 to 0.30 AU and increases beyond 0.30–1.01 AU. After the thickness reaches the inertial scale of the ions, the kinetic effects of the ions equilibrate the structure, and thus its thickness scales with the characteristic inertial length of the ion. For TDs, this characteristic scaling took place over the entire studied range from 0.06 to 1.01 AU. An analysis of the discontinuity thicknesses allowed observational confirmation that RDs are formed as a result of steepening of an Alfvén wave, while TDs are most likely the boundaries of magnetic tubes that approximately follow the theoretical Parker spiral.

Reference [100] presents the results of Solar Orbiter observations of the region of interaction between the jet and coronal plumes — filamentary ray structures extending from the chromosphere to the high corona, abundant in coronal holes and in quiet areas of the Sun and presumably giving rise to solar wind flows. The development of ripples and the disintegration of droplets were observed, which are associated with the development of Kelvin–Helmholtz instability and the appearance of a Karman vortex chain, two interrelated phenomena. The observed formation of vortices may represent a mechanism for mixing masses across the magnetic field and enhance the conversion of kinetic energy into thermal energy, heating the solar corona.

While previous space missions never approached closer than 60 solar radii to the Sun, the Parker Solar Probe approached to a distance of 9.5 solar radii and crossed the critical Alfvén surface several times, which separates the sub-Alfvén and super-Alfvén regions of the solar wind, i.e., it is considered the boundary between the solar corona, the plasma still associated with the Sun, and the free flow of the solar wind. As measurements have shown, this boundary is not spherical and is located at an average distance of 18.8 solar radii (13 million kilometers) from its photosphere. The measured Alfvén Mach number beneath the Alfvén surface was 0.79, and the magnetic pressure prevailed over the pressure of ions and electrons. The measurements were carried out over the region of a stable solar wind flow arising on rapidly expanding lines of the coronal magnetic field lying above the pseudo-streamer. The measured turbulence spectrum in the sub-Alfvén region is shown in Fig. 17. The break in the spectrum between the energy-containing range $1/f$

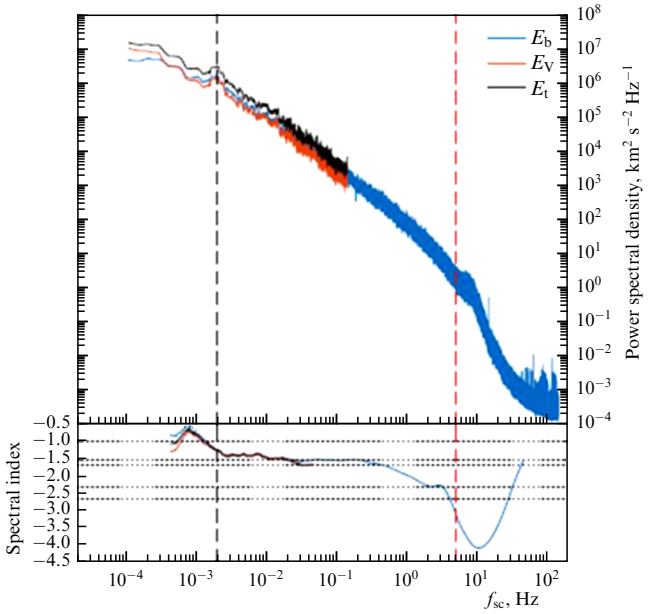

Figure 17. At top is power spectrum, at bottom is spectral index of magnetic (E_b), velocity (E_V), and total (E_t) fluctuations during 5 hours of Parker Solar Probe's stay in sub-Alfvénic region [101]. (Explanations in text.)

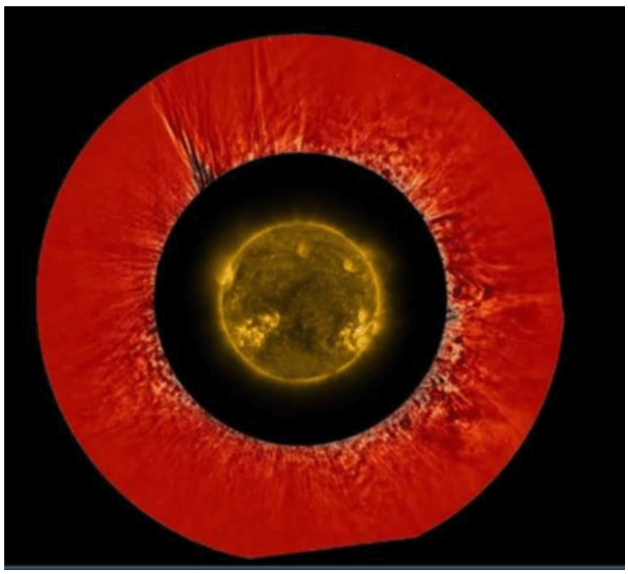

Figure 18. Detail of video observation of turbulence in lower corona (in red ring) by Metis/Solar Orbiter coronagraph, taken on October 12, 2022, from distance of 43.4 million km from Sun (less than a third of distance from Sun to Earth) [25].

(which in this case is smaller than $1/f_{sc}$,f_{sc} being the frequency in the spacecraft reference frame) and the inertial range $f_{sc}^{-3/2}$ was at a frequency of $f_{sc} \sim 2 \times 10^{-3}$ Hz and is indicated by a black dotted line. This break is associated with the outer scale, or the largest scale of fluctuations that can be attributed to turbulence. A small increase in spectral power is observed in the high-frequency part of the spectrum at ion-cyclotron frequencies (about 8 Hz), and then the spectrum drops sharply, not reaching the minimum noise level of the device [101]. For comparison with the measured spectrum, the horizontal dotted lines in the lower part of the figure correspond to spectral indices -1 for the $1/f$ spectrum and $-3/2$ and $-5/3$ for the model spectra of the inertial range of turbulence [102].

The Parker Solar Probe and Solar Orbiter made it possible to study the properties of plasma turbulence and solar wind in the corona and in the inner heliosphere at distances of 0.1–1 AU. The formation of turbulence near the Sun in the lower corona was observed on the Solar Orbiter with the Metis coronagraph (field of view of 1.7 $R_\odot$–9 $R_\odot$ [103]) (Fig. 18). These observations, obtained with high spatial resolution, showed that the motion of the solar wind in these regions already becomes chaotic, giving rise to fully developed turbulence in the solar corona [25].

Measurements by the Parker Solar Probe and Solar Orbiter in the inner heliosphere showed the presence of ion beams, plasma temperature anisotropy, and kinetic plasma waves, which, along with switchback phenomena, are considered kinetic mechanisms for heating and accelerating the solar wind and forming the spectrum of its turbulence [24, 104, 105]. Measurements of the properties of solar wind turbulence provided strong evidence of its radial evolution, namely, the evolution of solar wind plasma from super-Alfvén turbulence and a state of weakly developed turbulence near the Sun to intermediate and fully developed turbulence at a distance of 1 AU occurs [24. 106]. The study of the radial evolution of the turbulent nature of the plasma of the fast solar wind emanating from coronal holes, based on Parker Solar Probe and Solar Orbiter data, was carried out in [107] for heliospheric distances of 0.1–1 AU. Along with confirmation of a number of previously obtained results (a decrease in the radial trend of the proton density, which occurs more slowly than expected for a radially expanding plasma; deviation of the magnetic field from Parker's prediction; a slower decrease in the proton temperature relative to the adiabatic prediction; etc.), the expected decrease in the turbulence power level during expansion of the solar wind plasma and a power law for the spectral density of turbulence power in the inertial range between the Kolmogorov spectrum and Kraichnan scaling were discovered. The spectral index of the power spectral density of velocity fluctuations remained very close to the Iroshnikov–Kraichnan scaling at all radial distances, and the spectral index of magnetic field fluctuations decreased in absolute value with increasing radial distance from 0.1 to 0.97 AU. The same behavior of magnetic field fluctuations was also observed in the dissipative range, although with a steeper power law. It is noted that the slopes of the spectra in the frequency ranges from inertial to kinetic along the turbulent cascade strongly depend on the type of turbulence observed by the two spacecraft, namely, on predominantly parallel turbulence (along the magnetic field) in the Parker Solar Probe data and predominantly perpendicular turbulence in the Solar Orbiter data.

The radial dependences of various solar wind parameters obtained from data analysis are approximated by the following functions ($R_0 = 1$ AU) [107]:

— concentration of protons

$$n = (8 \pm 2)\left(\frac{R}{R_0}\right)^{(-1.8\pm0.2)} \text{ cm}^{-3},$$

— magnetic field amplitude

$$B = (5.3 \pm 0.4)\left(\frac{R}{R_0}\right)^{(-1.60\pm0.05)} \text{ nT},$$

— radial component of the magnetic field

$$|B_r| = (3.3 \pm 0.4)\left(\frac{R}{R_0}\right)^{(-1.72\pm0.09)} \text{ nT},$$

—tangential component of the magnetic field

$$|B_t| = (3.0 \pm 0.4)\left(\frac{R}{R_0}\right)^{(-1.4\pm0.1)} \text{ nT},$$

— temperature of protons

$$T = (1.7 \pm 0.1) \times 10^5\left(\frac{R}{R_0}\right)^{(-0.93\pm0.04)} \text{ K},$$

— plasma parameter

$$\beta = (1.58 \pm 0.08)\left(\frac{R}{R_0}\right)^{(0.49\pm0.04)}.$$

Based on the analysis of observational data, a statistical analysis of the current sheets and vortex-like structures detected at two radial distances was also performed, and it was found that these structures have similar characteristics at different radial distances.

The Parker Solar Probe crossed the edge of one of the magnetic loops at the base of a coronal mass ejection for the first time at a distance of only 14 solar radii, at which the structure of the ejection had not yet changed much due to its interaction with the interplanetary medium. Measurements showed a noticeable difference in the plasma parameters in the ejection from the parameters of the solar wind — an almost complete absence in the crossed part of the ejection of low-energy heavy and light ions (from hydrogen to iron), which are usually present in the surrounding plasma of the solar wind and in the head of the ejection. Such a difference in parameters may be associated with the rapid expansion of the magnetic loop at the base of the ejection during its injection into the corona and the cooling of superthermal ions [108]. A review of energetic particle measurements in the near-solar space using Parker Solar Probe/IS⊙IS (IS⊙IS — Integrated Science Investigation of the Sun) and Solar Orbiter/EPD (EPD — Energetic Particle Detector) data is given in [109]. It is noted that the approach of the spacecraft to the Sun, the source of particle acceleration, reduces the influence of transport effects on the characteristics of the particles and allows their acceleration conditions to be better determined. It was also found that the composition of particles from the same source in events occurring in rapid succession can vary greatly, and individual active regions can produce a series of ^{3}He-rich solar energetic particle events over a long period of time. These and other unexpected measurement results indicate different conditions in the acceleration region and require a revision of the generally accepted theories of energetic particle generation on the Sun and in the inner heliosphere.

In Ref. [110], the dynamics of energetic protons accelerated by an interplanetary collisionless shock wave in the November 3, 2021 event were analyzed using measurements from the Solar Orbiter (Electron-Proton Telescope sensor of the EPD suite), and constraints on the potential acceleration mechanisms and processes were considered. The analysis is based on a qualitative comparison of the obtained observations of such proton characteristics as pitch angle distribution, the time profile of the flux, and the distribution function of energetic protons by velocity near the shock wave with theoretical predictions. It was found that the time profile of protons with energies of $\sim 1000-4000$ keV rapidly increased and quickly decayed with a clear velocity dispersion approximately 2 min before the shock wave passage, similar to pulsed events of solar energetic particles. The peak energy spectrum of protons in this event was steeper than that at the shock wave itself. The fluxes of protons with energies of $\sim 50-200$ keV and with inverse velocity dispersion reached a maximum between ~ 10 and ~ 20 s before the shock wave passage, and the velocity dispersion and inverse velocity dispersion events were associated with the passage of the shock wave through magnetic bends (reverse switching phenomena). Two different proton populations were observed near the shock wave. In one of them, protons at energies below ~ 300 keV are characterized by a power-law spectrum with an index of ~ 6–7 and a flux time profile that increased before the shock wave and decreased after its passage. This proton population could be a continuation of superthermal protons with energies of $\sim 20-60$ keV and effectively accelerated by the shock wave. Another proton population above ~ 300 keV is a long-lived, solar-directed beam through the shock wave with a flux time profile that remains relatively constant before the shock wave and increases slightly after it passes. Such a proton beam could presumably originate from a solar source, and its observed characteristics could be explained by the inefficiency of proton acceleration by the shock wave at energies above ~ 300 keV, which is not the case for the very efficient acceleration in the velocity dispersion event. In this event, the flux time profile with a fast build-up and fast decay lasted $\lesssim 30$ s, which corresponds to a spatial scale of the order of the gyroradius of a ~ 1000-keV proton, and the observed duration may indicate that protons are accelerated in a pulsed way in a region comparable to the proton gyroradius on the shock wave surface. An inverse velocity dispersion event for protons with energies of ~ 50–200 keV was observed immediately before the shock wave and had a short duration of $\lesssim 15$ s, which suggests that its source is limited to a region comparable to the gyroradius of a proton with an energy of ~ 200 keV. This event was also associated with the passage of the shock wave through the magnetic bend, and such interaction between the magnetic bend and the shock wave likely results in the impulsive and efficient acceleration of protons in velocity dispersion events. The results obtained allow us to consider the drift and diffuse acceleration mechanisms to be acceleration mechanisms on interplanetary shock waves.

The heliocentricity of the Solar Orbiter orbit and the ability to observe the side of the Sun invisible from Earth made it possible, during a period of powerful events on the Sun in May 2024, associated with the active region AR3664, which produced a series of powerful flares on the visible disk, to monitor the flare activity of this region on the invisible side of the Sun, before the region reached the eastern limb, providing an advance forecast of space weather for several days ahead (3–4 days) and forestalling the negative consequences of the impact on radio communications and technical systems on Earth, which subsequently occurred. Crossing the coronal mass ejection, the Parker Solar Probe/IS⊙IS detected streams of energetic particles that go ahead of the coronal mass ejection with an interval of approximately one day (Fig. 19), which can be considered a precursor of the ejection itself, used to forecast space weather [24, 111].

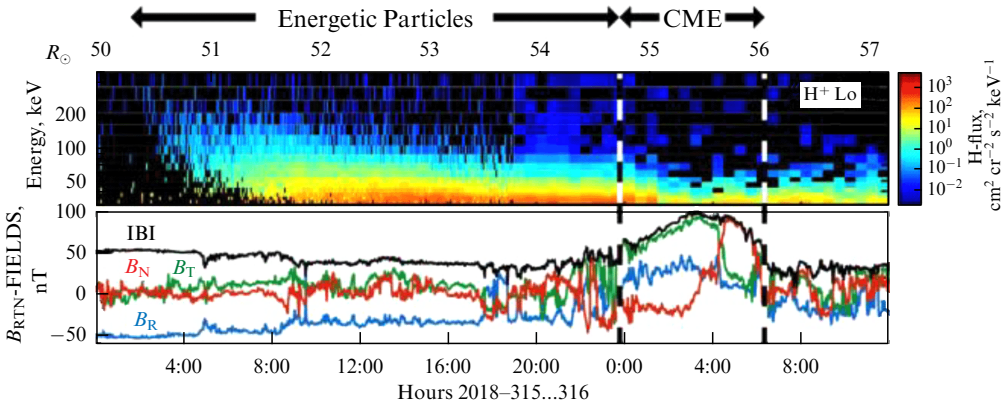

Figure 19. Proton flux is shown in color at top of figure, and magnetic field measurements of ejecta are shown at bottom [111] (Credit: NASA/ Goddard).

Shock wave interactions with coronal mass ejection (CME) sequences that are important for space weather forecasting have been described from Solar Orbiter, Wind, STEREO-A, ASO-S, and CHASE measurements [112]. Of the three successive CMEs that occurred on November 27–28, 2023, CME-3 was accompanied by a shock wave that successively compressed and modified the two preceding CMEs as it propagated. At distances close to the Sun, CME-1 and CME-2 interacted with each other, and at distances less than 0.83 AU, the shock wave overtook interplanetary CME-2 (ICME-2) and compressed it. Continuing to propagate, the shock wave crossed ICME-2, then ICME-1 (at a distance of 1 AU), and overtook both ejections, causing their compression, accompanied by an increase in the magnetic field strength ($\sim 150\%$) and a weakening of the shock wave strength (the degree of magnetic compression decreased from 1.74 to 1.49). Despite the observed noticeable interaction of the three ICMEs in the heliosphere, their magnetic structure was preserved at different observation points, especially for ICME-3.

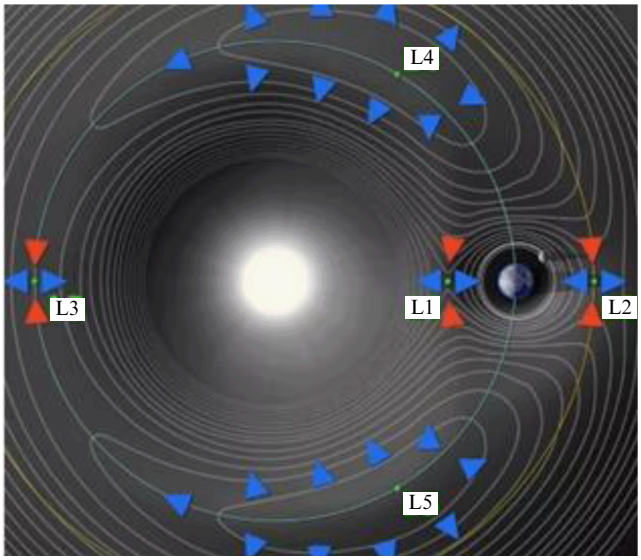

Figure 20. Diagram showing relative positions of Sun and Earth and five Lagrange points, with contour lines of effective potential (https://en.wikipedia.org/wiki/Lagrange_point).

6. Prospects

The upcoming NASA mission IMAP (Interstellar-Mapping and Acceleration Probe) will operate at the L1 Lagrange point (Fig. 20) of the Sun–Earth system and will carry 10 scientific instruments to study the heliosphere and the solar wind and its interaction with the interstellar medium, accelerate energetic particles, study energetic neutral atoms, and monitor space weather [113]. Jointly with the launch of this spacecraft is planned the launch of the SWFO-L1 (Space Weather Follow On-Lagrange 1) spacecraft [114], which, while at the L1 Lagrange point, will carry a set of instruments to measure the solar wind, energetic particles, and the magnetic field in real time, as well as a compact coronagraph [115] to detect coronal mass ejections. The mission's objective is to ensure reliable provision of information for monitoring and forecasting space weather in conditions where all spacecraft intended for these purposes have operated beyond their design life.

China plans to launch the Xihe-2 (Lagrange-V Solar Observatory (LAVSO)) spacecraft in 2026 for the first observations of the Sun from the L5 Lagrange point of the Sun–Earth system (see Fig. 20) [116, 117]. The main objectives are to study the generation and evolution of solar magnetic fields, their relationship with mass ejections, and the three-dimensionality of ejections and to provide accurate warning and forecasting of space weather. In 2029, it is planned to send the Xihe-3 space observatory from the ecliptic plane to study the solar poles and to obtain data on solar magnetic activity cycles and high-speed solar wind. An orbit with a large inclination to the ecliptic plane (about $60-70^\circ$) will be formed by a gravity assist maneuver near Jupiter. The information received from out-of-ecliptic sections of the orbit is intended to provide new insights into solar phenomena that affect space weather and Earth's technological infrastructure. The planned scientific equipment complex will include a block of remote instruments (a magnetic and helioseismic telescope, hard UV and X-ray telescopes, a white-light coronagraph and a wide-angle coronagraph, and a low-frequency radio spectrometer) and a set of instruments for local measurements (a solar wind ion analyzer, an energy ion analyzer, and a magnetometer) [118]. Close-range observations of the Sun are planned as part of the Xihe-4 mission under discussion [119].

The prospects for Russian space research of the Sun are associated with projects that have a certain groundwork in their development and which are constantly being modernized in terms of current scientific tasks and measuring equipment, taking into account the latest achievements in solar physics. The Arka project is aimed at X-ray observa-

tions of the Sun from near-Earth orbits with high spatial resolution to study the fine structure of the solar atmosphere and activity on small and ultra-small scales (75 km = 0.1″) and to study micro- and nanoflares, transient processes at the chromosphere-corona boundary, and heating of the solar corona. In the Interhelioprobe project [120], two spacecraft, separated by a quarter of the period and in orbits inclined to the plane of the ecliptic, will be able to provide continuous out-of-ecliptic observations of the polar regions of the Sun, and also, at the stage of approaching the Sun due to gravitational maneuvers near Venus, will observe the Sun with high spatial resolution, solving the problems of studying the trigger mechanisms of solar flares and mass ejections, the fine structure of the solar atmosphere, and its role in heating the solar corona and accelerating the solar wind. Experiments on observing the Sun from aboard the International Space Station (ISS) provide a certain backlog, the implementation stage of which can be transferred to the new ROS station. This is the Takhomag-ISS project, which consists of developing and testing a solar magnetograph for measuring magnetic fields on the Sun and for its use in solar space projects, as well as the CORTES project for developing new methods of X-ray observations of the Sun and for studying the solar corona, flares and pre-flare conditions, and the origin and evolution of eruptive phenomena. The Solntse-Terahertz project for studying terahertz radiation from the Sun is in the preparation stage for implementation on the ISS.

7. Conclusion

Observations and measurements with spacecraft have yielded new scientific results designed to solve problems in solar physics that are important for fundamental astrophysics and for practical problems of space weather, which has an increasing impact on various areas of human activity on Earth and in space. Current and planned space missions will allow us to take another important step towards a better understanding of how the Sun is structured and how it works, how distant stars may be structured, and how we can minimize the risks posed to us by space weather generated by solar activity. Many spacecraft observing the Sun in a wide range of the electromagnetic spectrum and with high spatial resolution are constantly moving us into ever smaller scales of the solar atmosphere, rapidly changing our understanding of the Sun, which provides a basis for developing new space missions.

It is not claimed that this review constitutes a complete presentation of the state and results of space research on the Sun, it aims to reflect only some of them on the 100th anniversary of S.I. Syrovatskii's birth.

References

1. Syrovatskii S I *Annu. Rev. Astron. Astrophys.* **19** 163 (1981)
2. Syrovatskii S I, in *Neutral Current Sheets in Plasmas* (Proc. (Trudy) of the P.N. Lebedev Phys. Inst., Vol. 74, Ed. N G Basov) (New York: Consultants Bureau, 1976) p. 1, https://doi.org/10.1007/978-1-4615-8564-0_1; Translated from Russian: *Neitral'nye Tokovye Sloi v Plazme* (Tr. Fiz. Inst. Akad. Nauk SSSR, Vol. 74, Ed. N G Basov) (Moscow: Nauka, 1974) p. 3
3. Syrovatskii S I, in *Vspyshechnye Protsessy v Plazme* (Flare Processes in Plasma) (Tr. Fiz. Inst. Akad. Nauk SSSR, Vol. 110, Ed. V L Ginzburg) (Moscow: Nauka, 1979) p. 5
4. Syrovatskii S I, Bulanov S V, Dogiel V A, in *Itogi Nauki i Tekhniki* (Results of Science and Technology) (Ser. Astronomy, Vol. 21) (Moscow: VINITI, 1982) p. 188;
5. Syrovatskii S I, Somov B V, in *Itogi Nauki i Tekhniki* (Results of Science and Technology) (Ser. Astronomy, Vol. 21) (Moscow: VINITI, 1982) p. 221
6. Syrovatskii S I, Zhugzhda Yu D *Sov. Astron.* **11** 945 (1968); *Astron. Zh.* **44** 1180 (1967)
7. Somov B V, Syrovatskii S I *Sov. Phys. Usp.* **19** 813 (1976); *Usp. Fiz. Nauk* **120** 217 (1976)
8. Syrovatskii S I, Shmeleva O P *Sov. Astron.* **16** 273 (1972); *Astron. Zh.* **49** 334 (1972)
9. Dogiel V A, Syrovatskii S I *Izv. Akad. Nauk SSSR Ser. Fiz.* **43** 716 (1979)
10. Kuznetsov V D, Syrovatskii S I *Sov. Astron.* **23** 715 (1979); *Astron. Zh.* **56** 1263 (1979)
11. Molodenskii M M, Syrovatskii S I *Sov. Astron.* **21** 734 (1977); *Astron. Zh.* **54** 1293 (1977)
12. Bobrova N A, Syrovatskii S I *Solar Phys.* **61** 379 (1979)
13. Syrovatskii S I *Sov. Astron. Lett.* **3** 69 (1977); *Pis'ma Astron. Zh.* **3** 133 (1977)
14. Kuznetsov V D, Syrovatskii S I *Solar Phys.* **69** 361 (1981)
15. Tsuneta S *Trends Sci.* **18** (11) 11_79 (2013) https://doi.org/10.5363/tits.18.11_79
16. A golden age of solar physics. The Royal Astronomical Society, https://ras.ac.uk/events-and-meetings/golden-age-solar-physics
17. "Solar Orbiter Exploring the Sun-heliosphere connection," Definition Study Report ESA/SRE(2011)14 (Frascati: European Space Agency, 2011); http://sci.esa.int/solar-orbiter/48985-solar-orbiter-definition-study-report-esa-sre-2011-14/#
18. Kuznetsov V D *Phys. Usp.* **49** 305 (2006); *Usp. Fiz. Nauk* **176** 319 (2006)
19. Kuznetsov V D, in *Pyat'desyat Let Kosmicheskikh Issledovanii: po Materialam Mezhdunarodnogo Foruma "Kosmos: Nauka i Problemy XXI Veka," Oktyabr' 2007 Goda, Rossiiskaya Akademiya Nauk, Moskva* (Fifty Years of Space Research: on the Materials of the Intern. Forum "Space, Science and Problems of the XXI Century," October 2007, Russian Academy of Sciences, Moscow) (Ed. A V Zakharov) (Moscow: Fizmatlit, 2009) p. 60
20. Kuznetsov V D *Phys. Usp.* **53** 947 (2010); *Usp. Fiz. Nauk* **180** 988 (2010)
21. Kuznetsov V D *Phys. Usp.* **55** 305 (2012); *Usp. Fiz. Nauk* **182** 327 (2012)
22. Kuznetsov V D, in *The CORONAS-F Space Mission. Key Results for Solar Terrestrial Physics* (Astrophysics and Space Science Library, Vol. 400, Ed. V Kuznetsov) (Berlin: Springer, 2014) p. 1, https://doi.org/10.1007/978-3-642-39268-9_1; Translated from Russian: *Solnechno-Zemnaya Fizika: Rezul'taty Eksperimentov na Sputnike KORONAS-F* (Ed. V D Kuznetsov) (Moscow: Fizmatlit, 2009) p. 10
23. Kuznetsov V D *Adv. Space Res.* **55** 879 (2015)
24. Parker Solar Probe. NASA Science, https://science.nasa.gov/mission/parker-solar-probe/
25. Solar Orbiter. The European Space Agency, https://www.esa.int/Science_Exploration/Space_Science/Solar_Orbiter
26. Li C et al. *Res. Astron. Astrophys.* **19** 165 (2019)
27. Advanced Space-based Solar Observatory (ASO-S), http://aso-s.pmo.ac.cn/en_index.jsp
28. ADITYA-L1. Indian Space Research Organisation, ISRO, https://www.isro.gov.in/Aditya_L1.html
29. Proba-3 Mission. The European Space Agency. ESA, https://www.esa.int/Enabling_Support/Space_Engineering_Technology/Proba_Missions/Proba-3_Mission3
30. Solar Dynamics Observatory. NASA, https://sdo.gsfc.nasa.gov/
31. Zhao J et al. *Astrophys. J. Lett.* **774** L29 (2013)
32. Hazra G, Karak B B, Choudhuri A R *Astrophys. J.* **782** 93 (2014)
33. Hathaway D H, Upton L, Colegrove O *Science* **342** 1217 (2013)
34. SOHO: Solar and Heliospheric Observatory. The European Space Agency, https://www.esa.int/Science_Exploration/Space_Science/SOHO
35. Requerey I S et al. *Astrophys. J.* **789** 6 (2014)
36. Bonet J A et al. *Astrophys. J. Lett.* **723** L139 (2010)
37. Okamoto T J, Sakurai T *Astrophys. J. Lett.* **852** L16 (2018)
38. Nölke J D et al. *Astron. Astrophys.* **678** A196 (2023)
39. Rao S et al. *Nat. Astron.* **8** 1102 (2024)
40. Jafarzadeh S et al. *Astron. Astrophys.* **688** A2 (2024)

41. Petrova E et al. *Astron. Astrophys.* **687** A13 (2024)
42. Kohutova P, Verwichte E, Froment C *Astron. Astrophys.* **633** L6 (2020)
43. Pariat E, Antiochos S K, DeVore C R *Astrophys. J.* **691** 61 (2009)
44. Hinode, http://hinode.nao.ac.jp/en/intro/science/discovery.html
45. De Pontieu B et al. *Publ. Astron. Soc. Jpn.* **59** (SP3) S655 (2007)
46. De Pontieu B et al. *Science* **331** 55 (2011)
47. Régnier S et al. *Astrophys. J.* **784** 134 (2014)
48. De Pontieu B et al. *Astrophys. J. Lett.* **845** L18 (2017)
49. De Pontieu B, Martínez-Sykora J, Chintzoglou G *Astrophys. J. Lett.* **849** L7 (2017)
50. Chintzoglou G et al. *Astrophys. J.* **857** 73 (2018)
51. De Pontieu B et al. *Solar Phys.* **296** 84 (2021)
52. Pontin D et al. *Astrophys. J.* **837** 108 (2017)
53. Cirtain J W et al. *Nature* **493** 501 (2013)
54. Aschwanden M J, Peter H *Astrophys. J.* **840** 4 (2017)
55. Barczynski K, Peter H, Savage S L *Astron. Astrophys.* **599** A137 (2017)
56. Rachmeler L A et al. *Solar. Phys.* **294** 174 (2019)
57. Williams T et al. *Astrophys. J.* **892** 134 (2020)
58. Alexander C E et al. *Astrophys. J. Lett.* **775** L32 (2013)
59. Alpert S E et al. *Astrophys. J.* **822** 35 (2016)
60. Tiwari S K et al. *Astrophys. J.* **816** 92 (2016)
61. The Sun. NuSTAR. Caltech, https://www.nustar.caltech.edu/page/sun
62. Warren H et al. *Astrophys. J.* **854** 122 (2018)
63. Li Y et al. *Astrophys. J. Lett.* **853** L15 (2018)
64. Chitta L P, Priest E R, Cheng X *Astrophys. J.* **911** 133 (2021)
65. Ding T et al. *Astrophys. J.* **964** 58 (2024)
66. Ding T, Zhang J *Astrophys. J.* **974** 104 (2024)
67. HMI Science Nuggets. Stanford Univ., http://hmi.stanford.edu/hminuggets/?p = 539
68. Battaglia A F et al. *Astron. Astrophys.* **691** A172 (2024)
69. The Solar Ultraviolet Imaging Telescope. Indian Space Research Organisation, https://www.isro.gov.in/Aditya_L1_SUIT.html
70. HEL1OS captures first High-Energy X-ray glimpse of Solar Flares. Indian Space Research Organisation, ISRO, https://www.isro.gov.in/HEL1OS_captures_glimpseof_solarflares.html
71. Indian spacecraft Aditya-L1 observes solar flare. Max-Planck-Gesellschaft, https://www.mpg.de/24282801/solar-probe-aditya-observes-flare
72. Historic First: India's Solar Ultra-violet Imaging Telescope (SUIT) onboard Aditya-L1 Captures Unprecedented Solar Flare Details. Indian Space Research Organisation, ISRO, https://www.isro.gov.in/SUIT_Aditya-L1_Captures_SolarFlare.html
73. Li S-Y et al. *Res. Astron. Astrophys.* **25** 015006 (2025)
74. Song Y et al. *Solar Phys.* **299** 85 (2024)
75. Gou T et al. *Solar Phys.* **299** 99 (2024); arXiv:2406.02783
76. Okamoto T J et al. *Astrophys. J.* **809** 71 (2015)
77. Antolin P et al. *Astrophys. J.* **809** 72 (2015)
78. Chitta L P et al. *Science* **381** 867 (2023)
79. Yardley S L et al. *Nat. Astron.* **8** 953 (2024)
80. Barczynski K et al. *Astron. Astrophys.* **673** A74 (2023)
81. Shibata K et al. *Science* **318** 1591 (2007)
82. Bale S D et al. *Nature* **576** 237 (219)
83. Kasper J C et al. *Nature* **576** 228 (219)
84. Zank G P et al. *Astrophys. J.* **903** 1 (2020)
85. Hatfield M, Thomas V "Switchbacks Science: Explaining Parker Solar Probe's Magnetic Puzzle," March 09, 2021, NASA, https://www.nasa.gov/science-research/heliophysics/switchbacks-science-explaining-parker-solar-probes-magnetic-puzzle/
86. Drake J F et al. *Astron. Astrophys.* **650** A2 (2021)
87. Huang J et al. *Astrophys. J.* **952** 33 (2023)
88. Squire J, Chandran B D G, Meyrand R *Astrophys. J. Lett.* **891** L2 (2020)
89. Goldstein M et al. *Radiat. Effects Defects Solids* **175** 1002 (2020)
90. Schwadron N A, McComas D J *Astrophys. J.* **909** 95 (2021)
91. Fedorov A et al. *Astron. Astrophys.* **656** A40 (2021)
92. Bandyopadhyay R et al. *Astron. Astrophys.* **650** L4 (2021)
93. Telloni D et al. *Astrophys. J. Lett.* **936** L25 (2022)
94. Horbury T S, Matteini L, Stansby D *Mon. Not. R. Astron. Soc.* **478** 1980 (2018)
95. Balogh A et al. *Geophys. Res. Lett.* **26** 631 (1999)
96. Yamauchi Y et al. *J. Geophys. Res. Space Phys.* **109** A03104 (2004)
97. Kieokaew R et al. *Astron. Astrophys.* **656** A12 (2021)
98. Kenny K N et al. *Astrophys. J.* **975** 283 (2024)
99. Madar A et al. *Astron. Astrophys.* **690** A328 (2024)
100. Wei H et al. *Astron. Astrophys.* **678** L7 (2023)
101. Kasper J C et al. *Phys. Rev. Lett.* **127** 255101 (2021)
102. Chen C H K *J. Plasma Phys.* **82** 535820602 (2016)
103. Antonucci E et al. *Astron. Astrophys.* **642** A10 (2020)
104. Ofman L et al. *Astrophys. J.* **926** 185 (2022)
105. Rivera Y J et al. *Science* **385** 962 (2024)
106. Telloni D et al. *Astrophys. J. Lett.* **912** L21 (2021)
107. Perrone D et al. *Astron. Astrophys.* **668** A189 (2022)
108. McComas D J et al. *Astrophys. J.* **943** 71 (2023)
109. Malandraki O E et al. *Phys. Plasmas* **30** 050501 (2023)
110. Yang L et al. *Astron. Astrophys.* **686** A132 (2024)
111. McComas D J et al. *Nature* **576** 223 (2019)
112. Chi Y et al. *Astrophys. J. Lett.* **975** L25 (2024)
113. Interstellar Mapping and Acceleration Probe (IMAP) mission at Princeton. Princeton Univ., https://imap.princeton.edu/
114. Space Weather Follow On L1 Mission. National Environmental Satellite, Data, and Information Service. National Oceanic and Atmospheric Administration, https://www.nesdis.noaa.gov/our-satellites/future-programs/swfo/space-weather-follow-l1-mission
115. Adkins J "NASA Awards Contracts for NOAA Coronagraph Instrument Phase A Study." May 01, 2023. NASA, https://www.nasa.gov/news-release/nasa-awards-contracts-for-noaa-coronagraph-instrument-phase-a-study/
116. Fang C et al. *Aerospace Shanghai* **41** (3) 9 (2024) https://doi.org/10.19328/j.cnki.2096-8655.2024.03.002; https://www.researching.cn/articles/OJ63ddd4526d92f09
117. "China to initiate 3D solar exploration as solar probing satellite Xihe-2 enters demonstration stage," Global Times, Sep. 15, 2023, https://www.globaltimes.cn/page/202309/1298241.shtml
118. Jones A "China to send a spacecraft out of the ecliptic to study the Sun's poles," Space News, February 25, 2025, https://spacenews.com/china-to-send-a-spacecraft-out-of-the-ecliptic-to-study-the-suns-poles/
119. Paradiso R "Xihe-2: the Sun and the Earth in a single glance," Space Voyaging, Sep. 21, 2023, https://www.spacevoyaging.com/news/2023/09/21/xihe-2-the-sun-and-the-earth-in-a-single-glance/
120. Kuznetsov V D et al. *Geomagn. Aeronomy* **56** 781 (2016)